

## Corrosion behaviour of plastically deformed high-Mn austenitic steels

**A. Grajcar\***, **W. Krukiewicz**, **S. Kołodziej**

Division of Constructional and Special Materials, Institute of Engineering Materials and Biomaterials, ul. Konarskiego 18A, 44-100 Gliwice, Poland

\* Corresponding author: E-mail adam.grajcar@polsl.pl

Received 12.09.2010; published in revised form 01.11.2010

### Properties

#### ABSTRACT

**Purpose:** The aim of the work was the comparison of corrosion resistance in an aqueous sulfuric acid solution of two high-manganese austenitic steels of the 0.05C-25Mn-Al-Si-Nb-Ti type in a plastically deformed state.

**Design/methodology/approach:** Investigations were carried out on specimens obtained from a thermo-mechanically rolled sheet and then plastically deformed through bending and immersed in corrosive solutions (1N H<sub>2</sub>SO<sub>4</sub>) for 100 hours. The mass decrement was calculated by the gravimetric method, whereas the character of corrosion damages was observed in metallographic investigations using light and scanning electron microscopes both in the polished and etched states.

**Findings:** It was found that after the thermo-mechanical processing one steel is characterized by an austenitic structure with numerous annealing twins, whereas in the second steel lamellar martensitic phases in an austenitic matrix occur. The investigations showed that the examined high-manganese steels have very low corrosion resistance in normal H<sub>2</sub>SO<sub>4</sub>. Higher impact on the corrosion resistance than the phase composition has the chemical composition. The mass decrement of the steel with martensite plates is a bit higher than that with

a single-phase austenitic matrix. The specimens were intensively dissolved due to general corrosion accompanying by pitting and hydrogen cracking.

**Research limitations/implications:** To investigate in more detail the corrosion behaviour of high-manganese austenitic steels, the polarization tests and the analysis of corrosion products should be carried out.

**Practical implications:** The obtained results can be used for searching the appropriate way of improving the corrosion resistance of high-strength high-manganese austenitic steels.

**Originality/value:** The corrosion resistance of two types of advanced high-manganese austenitic steels with different initial structures was compared. Hydrogen impact in austenitic steels was discussed.

**Keywords:** Corrosion resistance; high-manganese steels; gravimetric method; pitting corrosion; general corrosion; hydrogen cracking

#### Reference to this paper should be given in the following way:

A. Grajcar, W. Krukiewicz, S. Kołodziej, Corrosion behaviour of plastically deformed high-Mn austenitic steels, Journal of Achievements in Materials and Manufacturing Engineering 43/1 (2010) 228-235.

## 1. Introduction

High manganese steels with austenitic structure belong to a group of advanced high strength steels for automotive industry [1]. Their particular beneficial connection of high strength, good plasticity and the ability to energy absorption of construction elements with suitable cross-sections, are a result of the great susceptibility of  $\gamma$  phase to plastic deformation during which dislocation glide, mechanical twinning or strain-induced martensitic transformation can occur. Besides 15-30% Mn, high-manganese steels include 0.03-1% C, 1-4% Si, 1-8% Al [1-5]. Mechanical properties of these steels depend on structural processes occurring during cold plastic deformation, which are highly dependent on SFE (Stacking Fault Energy) of austenite [3]. If it is from 12 to 20 mJm<sup>-2</sup>, a partial transformation of austenite into martensite occurs, taking advantage of TRIP (Transformation Induced Plasticity) effect. Values of SFE equal from 20 to 60 mJm<sup>-2</sup> determine intense course of mechanical twinning connected to TWIP effect (Twinning Induced Plasticity) [4]. Utilization of these phenomena allows to achieve mechanical properties of high-manganese steels in a wide range, i.e.  $YS_{0.2} = 250-400$  MPa, UTS = 500-1000 MPa, UEI = 30-70% [4-6].

Up to now the mean area of studies on high manganese steels was their high-temperature deformation resistance [2, 5-7] and especially, the cold-working behaviour [1, 3, 4, 8, 9]. Less attention has been paid on the corrosion resistance of these steels [10-16]. In the eighties of the last century, some investigations [8, 9] on Fe-C-Mn-Al alloys for cryogenic application were carried out in order to replace expensive Cr-Ni austenitic steels. The role of manganese boils to Ni replacement and obtaining austenitic microstructure, whereas aluminium has a similar impact as chromium. Performed studies [9] showed, that Fe-C-Mn-Al steels show inferior corrosion resistance than Cr-Ni steels and they can be used as a substitute only in some applications. Zhang and Zhu [10] reported that addition of 25% Mn to mild steel was very detrimental to the corrosion resistance in aqueous solutions. The Fe-25Mn alloy was difficult to passivate, even in such neutral aqueous electrolytes as 1M Na<sub>2</sub>SO<sub>4</sub> solution. They further reported, that the addition of 5% Al to Fe-25Mn, results in forming of a stable passivation region on the anodic polarization curves in Na<sub>2</sub>SO<sub>4</sub> solution, but there is still no passivation in 3.5% NaCl solution [10]. Low corrosion resistance of high-manganese steels in chloride solutions was confirmed by our preliminary results of potentiodynamic tests on Fe-0.05C-25Mn-3.5Si-1.5Al steel [11].

Recently, corrosion resistance of Fe-0.05-29Mn-3.1Al-1.4Si steel in acidic (0.1M H<sub>2</sub>SO<sub>4</sub>) and chloride containing (3.5% NaCl) environments was investigated by Kannan et. al. [12]. Moreover, they compared the corrosion behaviour of the tested steel with IF-type (Interstitial-Free) steel. On the basis of gravimetric tests and anodic polarization curves they found [12], that Fe-Mn-Al-Si steel has lower corrosion resistance than the IF steel, both in acidic and chloride media. However, the corrosion resistance of high manganese steel in chloride solutions is considerably higher than in acidic solutions.

Described results of corrosion tests concern steels in the annealed or supersaturated state. The influence of cold plastic deformation on behaviour of Fe-0.5C-29Mn-3.5Al-0.5Si steel in 3.5% NaCl was studied by Ghayad et. al. [14]. They showed, on the basis of potentiodynamic tests, that the steel shows no tendency to

passivation, independently on the steel structure after heat treatment (supersaturated, aged or strain-aged). Higher corrosion rate of deformed specimens than that of specimens in supersaturated state, was a result of faster steel dissolution caused by annealing twins, which show a different potential than the matrix. The highest corrosion rate was observed in strain-aged samples, as a result of ferrite formation, which creates a corrosive galvanic cell with the austenitic matrix [14].

Studies on the corrosion resistance of high-manganese steels are confined to following alloy types: Fe-Mn, Fe-Mn-Al and Fe-Mn-Al-Cr. There are no results concerning steels with increased silicon content. Initial structural examinations of Fe-0.05-25Mn-3.5Si-1.6Al-Ti-Nb steel [6, 11] showed, that the austenitic matrix contains some fraction of martensite  $\epsilon$  with a lamellar shape. The presence of martensite is a result of the decrease of austenite SFE, reached by adding Si and also, to some extent, Ti and Nb, which are fixing carbon and nitrogen, resulting in a decrease of  $\gamma$  phase stability. It was preliminary found [15], that the presence of the second, lamellar phase, has a slight impact on the corrosion progress acceleration in acidic and chloride media, but it is the reason of local microcracks, spreading out usually from non-metallic inclusions. Taking it into account, the aim of the present work is to determine the influence of cold plastic deformation on corrosion behaviour of two steels with single-phase austenitic structure and containing some fraction of  $\epsilon$  martensite in aqueous solution of sulphur acid.

## 2. Experimental procedure

Examinations were carried out on two high-manganese steels, vacuum melted in the Institute for Ferrous Metallurgy in Gliwice. The chemical composition of the investigated steels is presented in Table 1. The steels are characterized by similar C and Mn content. Significant impact on SFE of austenite has the difference in Al, Si and Ti concentration. A lower SFE of 24.5Mn-3.5Si-1.5Al-Nb-Ti steel compared to 26Mn-3Si-3Al-Nb-Ti steel is a result of the higher Si and lower Al content. Moreover, much larger Ti content in a first steel provides a decrease of  $\gamma$  phase stability, as a result of fixing the total nitrogen and a part of carbon [6].

Table 1.  
Chemical composition of the investigated steels

Component	Mass contents, (%)	
	26Mn-3Si-3Al-Nb-Ti	24.5Mn-3.5Si-1.5Al-Nb-Ti
C	0.065	0.054
Mn	26.0	24.4
Si	3.08	3.49
Al	2.87	1.64
P	0.004	0.004
S	0.013	0.016
Nb	0.034	0.029
Ti	0.009	0.075
N	0.0028	0.0039
O	0.0006	0.0006
Initial structure [6, 15]		
	$\gamma$	$\gamma+\epsilon+\alpha'$

The material used for the investigation was delivered in a form of segment of steel sheet with following dimensions 340x225x3.2 mm, obtained after hot rolling using the thermo-mechanical treatment method. The thermo-mechanical processing of studied steels consisted of:

- heating of a charge up to the temperature of 1100°C and austenitizing for 15 minutes,
- rolling of the charge in a temperature range from 1050°C to 850°C, according to conditions in Table 2,
- isothermal holding of a rolled sheet segments at the temperature of finishing rolling for 15s,
- solution heat treatment of the flat specimens in water.

Table 2.  
Rolling schedule for the flats with a thickness of 5.4 mm

Pass number	Deformation temperature, °C	Thickness before the pass, mm	Thickness after the pass, mm	Relative reduction, %
1	1050	5.4	4.3	20
2	950	4.3	3.7	15
3	850	3.7	3.2	15

Taking into account the high deformation resistance during hot-working [5-7], the relative reductions during rolling were equal from 20 to 15%. In these conditions, the process controlling the work hardening during the last rolling pass at a temperature of 850°C was the dynamic recovery [5, 6]. The corrosion test results of investigated steels in the thermo-mechanically processed state were described in [15]. In the current work, the corrosion resistance in a cold plastically-deformed state was investigated. Samples with a size of 10x15mm and a thickness between 3.1 and 3.2 mm were plastically deformed in room temperature trough bending to an angle of 90°, with a bending radius of 3mm. Before immersion into the corrosive solutions, the samples were ground to the 1000-grit finish, washed in distilled water and ultrasonically cleaned in acetone. Corrosion resistance of investigated steels was assessed using the gravimetric method, by immersing the samples into 1N H<sub>2</sub>SO<sub>4</sub> solution for 100 hours. Before the test, the specimens were weighed with an accuracy of 0.01 g. The temperature of the test was equal 23±1°C. After the test, the samples were secondly weighed. The percentage mass decrement was determined as follows:

$$m_p = \frac{m_i - m_f}{m_i} \cdot 100\% = \frac{m_d}{m_i} \cdot 100\% \quad (1)$$

where:  $m_p$  – percentage mass decrement [%],  $m_i$  – initial mass [g],  $m_f$  – final mass [g],  $m_d$  – mass decrement [g].

The corrosion rate was calculated using following formula:

$$V_{cor} = \frac{m_d}{S \cdot t} \text{ [g/m}^2 \text{ day]} \quad (2)$$

where:  $V_{cor}$  – corrosion rate [g/m<sup>2</sup> day],  $S$  – surface of a sample [m<sup>2</sup>],  $t$  – time of the measurement [day],  $m_d$  – mass decrement [g].

Metallographic observations of non-metallic inclusions and corrosion pits were carried out on polished sections, whereas the microstructure observations on specimens etched in nital. The

investigations were performed on LEICA MEF 4A light microscope, with magnifications from 100 to 1000x. Fractographic investigations were carried using scanning electron microscope SUPRA 25 (Zeiss) at the accelerating voltage of 20kV. In order to remove corrosion products, the specimens were ultrasonically cleaned before the analysis. Confirmation of a phase structure of the investigated steels in the initial state was carried out by the X-ray phase analysis, what was reported elsewhere [6, 15].

### 3. Results

The structures of the investigated steels after the thermo-mechanical treatment are shown in Figs. 1 and 2. The 26Mn-3Si-3Al-Nb-Ti steel exhibits a homogeneous austenite structure with grains elongated in the rolling direction (RD) (Fig. 1). The susceptibility to twinning confirms the presence of a great number of annealing twins. The lower stacking fault energy of the 24.5Mn-3.5Si-1.5Al-Nb-Ti steel results in the presence of the second phase with a lamellar shape, distributed in the austenite matrix (Fig. 2). The X-ray diffraction analysis performed in [6, 15] confirmed also the presence of  $\epsilon$  and  $\alpha'$  martensites, confirming low stacking fault energy of the steel. Martensite  $\alpha'$  has also a lamellar shape and its unequivocal distinction from lamellas of  $\epsilon$  phase is complicated. Usually, privileged places for martensite  $\alpha'$  forming are crossings of  $\epsilon$  martensite lamellas [8, 16]. This matter will be the topic of future studies. In both steels, immersed after deformation in 1N H<sub>2</sub>SO<sub>4</sub> many corrosion pits of various size were observed (Fig. 3). The amount and the size of pits are very high and they are formed along entire surface of the specimens. Privileged places to pits creation are concentrations of non-metallic inclusions, which are also probable place of hydrogen penetration. Hydrogen also penetrates deeper into the steel, accumulating usually in a surroundings of elongated non-metallic sulfide inclusions (Fig. 4).

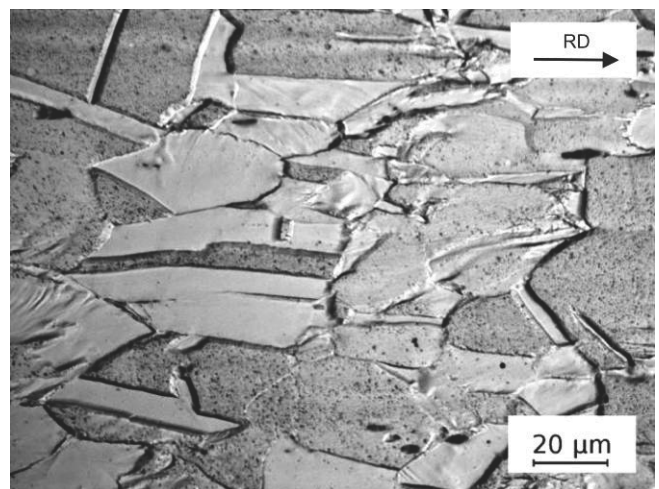


Fig. 1. Austenitic structure with annealing twins of 26Mn-3Si-3Al-Nb-Ti steel in the initial state (transverse section)

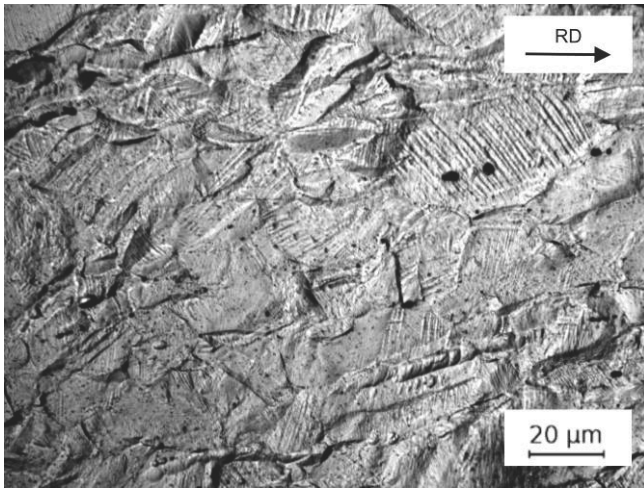


Fig. 2. Austenitic structure containing lamellar martensite plates, annealing twins and non-metallic inclusions of 24.5Mn-3.5Si-1.5Al-Nb-Ti steel in the initial state (transverse section)

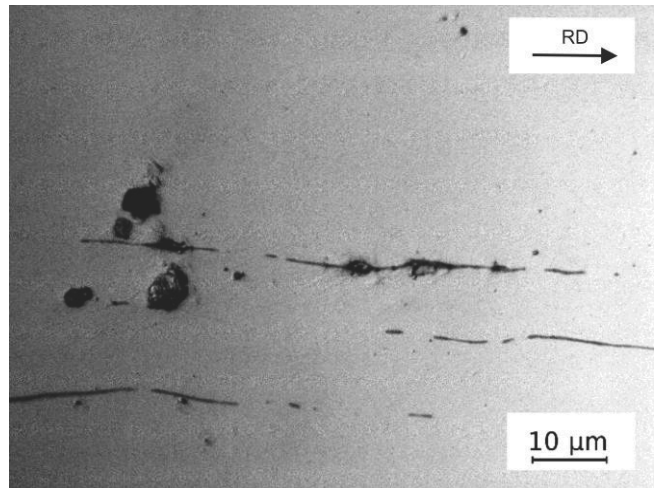


Fig. 4. Regions of hydrogen accumulation around elongated sulfide-type non-metallic inclusions in 24.5Mn-3.5Si-1.5Al-Nb-Ti steel (transverse section)

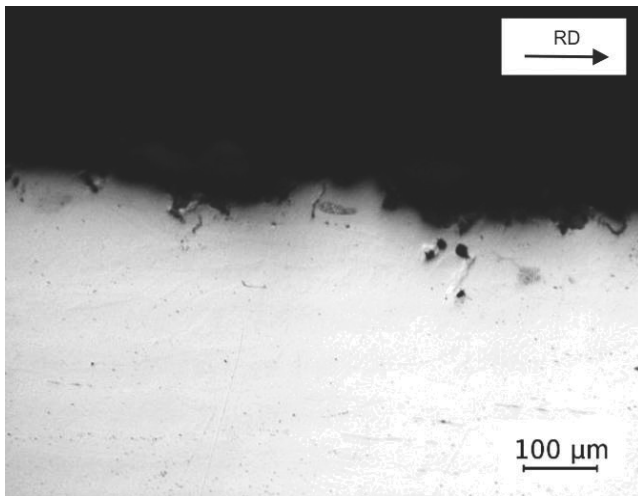


Fig. 3. Wide corrosion pits on the surface of 26Mn-3Si-3Al-Nb-Ti steel immersed in 1N H<sub>2</sub>SO<sub>4</sub> and probable places of hydrogen penetration (transverse section)

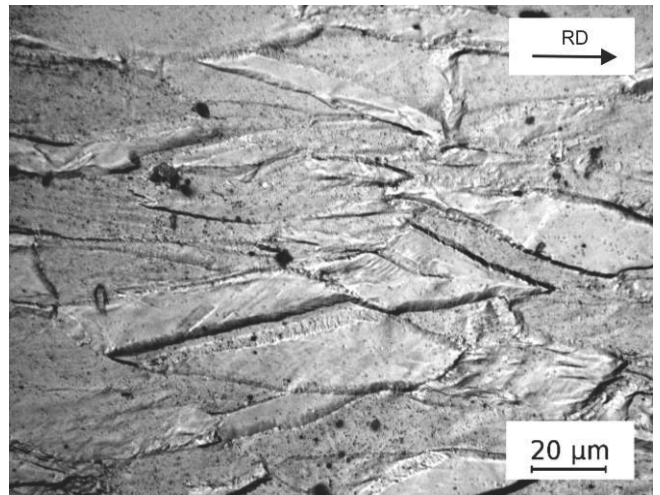


Fig. 5. Elongated austenite grains of 26Mn-3Si-3Al-Nb-Ti steel after cold plastic deformation and some places of hydrogen accumulation (transverse section)

Hydrogen failures were usually observed to the depth of about 0.3 mm. Places of hydrogen accumulation are also visible on samples revealing the steel structure after cold plastic deformation. Usually, these places are elongated non-metallic inclusions and grain boundary areas (Fig. 5). The 26Mn-3Si-3Al-Nb-Ti steel keeps after plastic deformation the austenitic structure, whereas a fraction of martensite in 24.5Mn-3.5Si-1.5Al-Nb-Ti steel is increasing (Fig. 6).

Besides non-metallic inclusions, especially privileged to hydrogen accumulation are lamellar areas of  $\epsilon$  martensite.

Absorbed atomic hydrogen penetrating the steel, accumulates in places with non-metallic inclusions, lamellar precipitations of the second phase, microcracks and other structural defects, where convenient conditions for recombining of atomic hydrogen to molecular H<sub>2</sub> exist. The recombination of atomic hydrogen to molecular state is a very exothermic reaction, which provides a pressure increase in formed H<sub>2</sub> bubbles as well as nucleation and growth of microcracks (Fig. 6) [17-19].

The results of the gravimetric test in acidic medium are listed in Table 3.

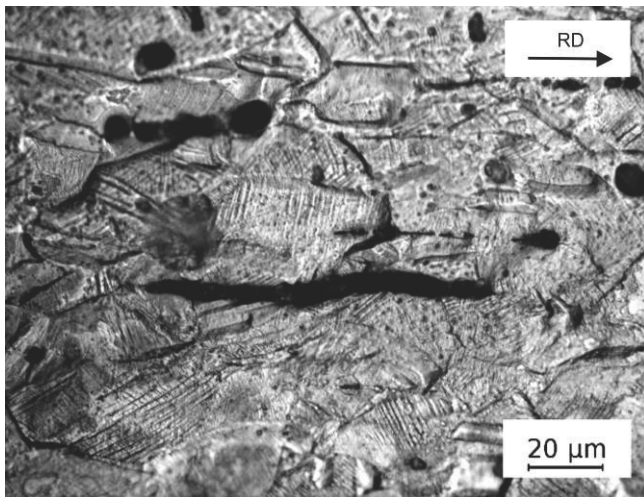


Fig. 6. Regions of hydrogen failures and hydrogen microcracks in 24.5Mn-3.5Si-1.5Al-Nb-Ti steel, plastically deformed and immersed in 1N H<sub>2</sub>SO<sub>4</sub> (transverse section)

Table 3. Results of gravimetric analysis for the specimens immersed in 1N H<sub>2</sub>SO<sub>4</sub>

26Mn-3Si-3Al-Nb-Ti			
m <sub>i</sub> , g	m <sub>f</sub> , g	m <sub>d</sub> , g	V <sub>cor</sub> , g/m <sup>2</sup> day
3.12	1.57	1.55	842.4
3.37	1.83	1.54	837.0
3.25	1.71	1.54	837.0
24.5Mn-3.5Si-1.5Al-Nb-Ti			
m <sub>i</sub> , g	m <sub>f</sub> , g	m <sub>d</sub> , g	V <sub>cor</sub> , g/m <sup>2</sup> day
3.76	1.92	1.84	1000.0
3.82	2.03	1.79	972.8
3.91	1.85	2.06	1119.6

After cold plastic deformation and 100 hours immersion in 1N H<sub>2</sub>SO<sub>4</sub> both steels show a meaningful percentage mass decrement, among 47 and 49% (Table 4).

Table 4. Percentage mass decrement of non-deformed specimens [15] and immersed in corrosion solutions after cold plastic deformation, %

Before cold deformation [15]	
26Mn-3Si-3Al-Nb-Ti	24.5Mn-3.5Si-1.5Al-Nb-Ti
38.4±5.2	41.3±9.6
After cold deformation	
26Mn-3Si-3Al-Nb-Ti	24.5Mn-3.5Si-1.5Al-Nb-Ti
47.5±1.6	49.5±2.4

Comparable mass decrement of two steels both in non-deformed and plastically deformed states indicates that the initial structure does not have any meaningful impact on the corrosion progress, which is 838 and 1030 g/m<sup>2</sup> day - correspondingly for the single-phase steel and the steel containing martensite plates.

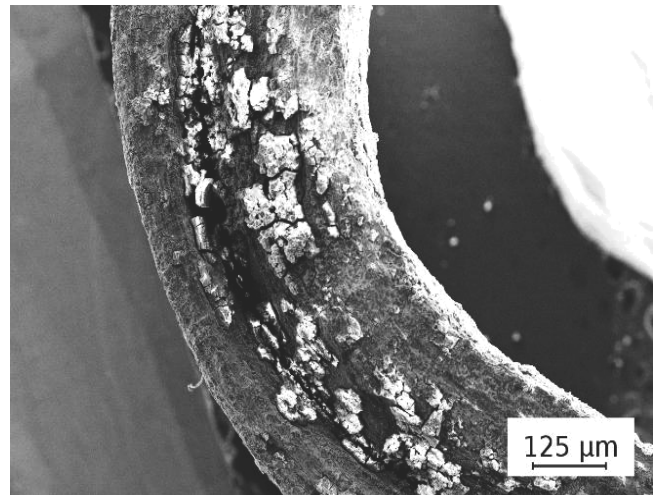


Fig. 7. Deep corrosion decrements and banding-like arrangement of corrosion products in 26Mn-3Si-3Al-Nb-Ti steel, plastically deformed and immersed in 1N H<sub>2</sub>SO<sub>4</sub>

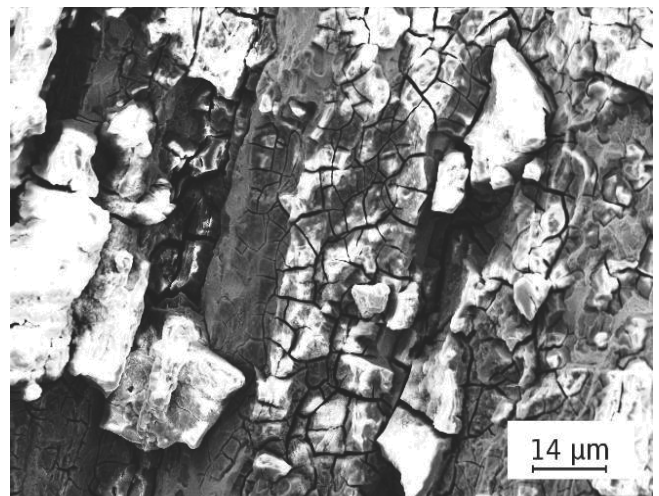


Fig. 8. Cracked layer of corrosion products with banding-like arrangement in 24.5Mn-3.5Si-1.5Al-Nb-Ti steel, plastically deformed and immersed in 1N H<sub>2</sub>SO<sub>4</sub>

Cold plastic deformation rises the mass decrement, in comparison with specimens investigated in undeformed state (Table 4) [15]. The high rate of corrosion progress of high-manganese steels in acidic solution is a result of hydrogen depolarization mechanism.

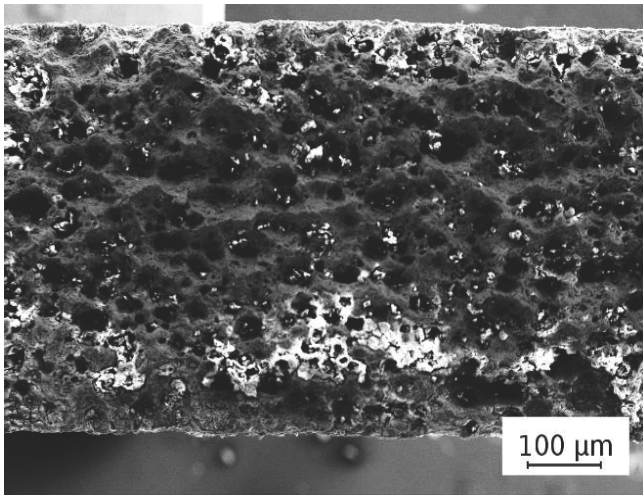


Fig. 9. Numerous craters formed due to corrosion pitting and probable hydrogen penetration in 26Mn-3Si-3Al-Nb-Ti steel, plastically deformed and immersed in 1N H<sub>2</sub>SO<sub>4</sub>

A precise definition of the character of corrosion damages was possible on the basis of scanning electron microscope observations. It is characteristic that corrosion cracks were not observed, whereas deep corrosion damages and band arranged corrosion products were perceived (Fig. 7). The corrosion products layer is not continuous and has many cracks (Fig. 8).

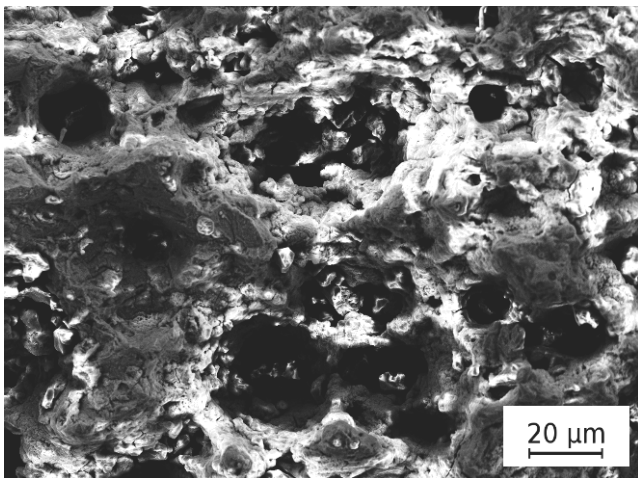


Fig. 10. Craters created as a result of corrosion pitting and probable hydrogen accumulation and corrosion products residues in 26Mn-3Si-3Al-Nb-Ti steel after the immersion test in 1N H<sub>2</sub>SO<sub>4</sub>

Besides remaining corrosion products, a numerous number of craters, created due to corrosion pitting and probably as a result of hydrogen impact, is characteristic. They are forming both in steel with martensite  $\epsilon$  lamellas and in steel with single-phase austenitic structure (Fig. 9). Similar craters and corrosion products residues were observed in the specimens immersed in 1N H<sub>2</sub>SO<sub>4</sub> - not subjected to cold deformation (Fig. 10).

## 4. Discussion

The obtained results confirmed the low corrosion resistance of high-manganese steels in acidic medium. The mass decrement in 1N H<sub>2</sub>SO<sub>4</sub> is near 50% (Table 4) and is more than 2 times of magnitude higher in comparison with samples investigated earlier in chloride solution [15]. A similar order of magnitude of corrosion progress was observed for Fe-0.05C-30Mn-3Al-1.4Si steel by Kannan et. al. [12], which showed that the corrosion current values in acidic solution are more than 2 orders of magnitude higher than in chloride solution. The plastic deformation enhances a higher corrosion rate compared to undeformed specimens (Table 4) [15].

Big dissimilarities in corrosion resistance of examined steels in different solutions are due to a different corrosion mechanism. The big mass loss in H<sub>2</sub>SO<sub>4</sub> solution is due to the hydrogen depolarization progress. This is a process of reduction (in cathodic areas) of hydrogen ions (from the electrolyte) by electrons (from the metal), to gaseous hydrogen, accelerating the corrosion progress [20, 21]. In this process numerous, wide and deep corrosion pits are forming (Fig. 3). Especially intensive corrosion pits form in places containing non-metallic inclusions, which are more resistant than the rest of material and foster potential differences and galvanic cell creation. This causes the absorption of hydrogen ions, which due to increasing pressure and temperature, recombine to a gaseous form and get out of the metal creating characteristic craters (Figs. 9, 10).

Hydrogen Induced Cracking (HIC) is a problem in carbon steels and especially in high-strength low-alloy steels. Typical examples are hydrogen failures of gas pipelines containing hydrogen sulfite [17-22, 25]. Conventional Cr-Ni austenitic steels are not usually liable to such damages. One of the reasons is relatively low diffusion coefficient of hydrogen in austenite as distinguished from steels with ferritic or martensitic structures [23-25]. However, enhanced permeation of hydrogen was observed in cold worked austenitic steels what was attributed to strain-induced martensitic transformation leading to promote hydrogen diffusion as the diffusivity is much higher in the bcc martensite lattice [23]. Additionally, hydrogen mobility is enhanced in the presence of high-dislocation density due to cold working [26]. It is important to note that hydrogen impact occurs both in diphas (Figs. 4, 6) and single phase (Figs. 9, 10) structures of the steels. In the investigated high-manganese austenitic steels a high corrosion rate (Table 3) and uncovering of metal surface by formed successively corrosion pits (Fig. 3) should be taken into account. Uncovered active metal inside of expanding pits reacts with the acidic solution with hydrogen emission [21]. In this regard hydrogen impact can influence the corrosion behaviour of the investigated high-manganese steels. Indirect confirmation of this fact are numerous craters formed due to corrosion pitting and probably hydrogen impact (Figs. 9, 10). The effect of hydrogen can be further enhanced by the presence of increased sulphur concentration (for example present as sulfide non-metallic inclusions) [21].

Craters forming is accompanied by local cracking of corrosion products layer (Figs. 7, 8), uncovering the metal surface and causing further penetration of the corrosive medium and finally the intensive progress of general corrosion. Corrosion products show the characteristic layout consistent with the

deformation direction (Fig. 7). Places of hydrogen accumulation are mostly the non-metallic inclusions, grain boundary areas and martensite lamellas near sheet surface (Figs. 4-6). Recombination of atomic hydrogen to the molecular state provides a pressure increase in formed  $H_2$  bubbles and creation of hydrogen cracks, especially close to martensite plates of high hardness (Fig. 6) [15].

The mass decrement in both steels is comparable (Table 4). It concerns both non-deformed and cold deformed specimens. It indicates, that martensite plates do not have any meaningful impact on the corrosion progress. This is probably due to the fact, that martensite  $\epsilon$  and  $\alpha'$  are diffusionless products of austenite transformation and have the same chemical composition like the steel matrix. An acceleration of the corrosion progress occurs in steels with some ferrite fraction (with different chemical composition than  $\gamma$  phase), formed during strain-aging of samples which were previously plastically deformed [14]. Therefore, the corrosion susceptibility of high-manganese steels is rather related to the chemical composition than to the phase structure. In general, the low corrosion resistance of high-manganese steels is coming from the fact, that manganese forms on the surface not very stable manganese oxides due to its low passivity coefficient [12]. This leads in consequence to high-speed dissolution of Mn and Fe atoms, especially intensive in sulphur acid solution. The corrosion progress in chloride media is much smaller [11-15]. The chemical composition influence is confirmed by the lower mass decrement of the steel with a higher aluminum content (Table 4).

The high mass decrement of steels examined in  $H_2SO_4$  solution is a result of fast general corrosion progress, enhanced by formation of corrosion pits (Fig. 3). Moreover, Ghayad et. al. [14] point the role of mechanical twins created during cold plastic deformation, as a factor which accelerates the corrosion progress. This is confirmed by the higher mass decrement of specimens subjected to bending compared to undeformed specimens, only dipped in 1N  $H_2SO_4$ . The role of mechanical twins in the investigated steels requires further examinations.

## 5. Conclusions

The corrosion resistance investigations were carried out on two high-manganese steels with a different structural state in an aqueous sulphur acid solution. The steel of higher aluminum concentration has a single-phase austenitic structure with many annealing twins and the second steel contains some fraction of martensitic phases of lamellar morphology. In particular it was found that:

- the percentage mass decrement of plastically deformed specimens immersed in 1N  $H_2SO_4$  for 100 hours is equal about 50% and is higher compared to non-deformed specimens;
- the percentage mass decrement in the steel with single-phase austenitic structure is slightly lower than in the steel containing  $\epsilon$  and  $\alpha'$  martensite lamellas. However, any significant impact of the second phase on corrosion process acceleration was not observed;
- the decisive impact on the corrosion resistance of examined steels has their chemical composition, which determines the high speed of Mn and Fe dissolution in acidic media. The intense dissolution of steels is a result of general corrosion

accompanied by formation of corrosion pits;

- the surface layer of band-arranged corrosion products located accordingly to the deformation direction has many cracks especially in surroundings of corrosion pits;
- a higher mass decrement of 24.5Mn-3.5Si-1.5Al-Nb-Ti steel is probably a result of the lower aluminum content compared to 26Mn-3Si-3Al-Nb-Ti steel;
- identified craters are combined effect of various corrosion damages in high-manganese austenitic steels. Hydrogen impact is an additional effect accompanying general corrosion and corrosion pits forming. Its influence is enhanced by numerous corrosion pits, sulfide non-metallic inclusions and martensite plates of high hardness.

## References

- [1] G. Frommeyer, U. Br ux, P. Neumann, Supra-ductile and high-strength manganese-TRIP/TWIP steels for high energy absorption purposes, *ISIJ International* 43 (2003) 438-446.
- [2] B. Wietbrock, M. Bambach, S. Seuren, G. Hirt, Homogenization strategy and material characterization of high-manganese TRIP and TWIP steels, *Materials Science Forum* 638-642 (2010) 3134-3139.
- [3] S. Allain, J-P. Chateau, D. Dahmoun, O. Bouaziz, Modeling of mechanical twinning in a high manganese content austenitic steel, *Materials Science and Engineering A* 387-389 (2004) 272-277.
- [4] O. Gr ssel, L. Kr ger, G. Frommeyer, L.W. Meyer, High strength Fe-Mn-(Al, Si) TRIP/TWIP steels development – properties - application, *International Journal of Plasticity* 16 (2000) 1391-1409.
- [5] L.A. Dobrzański, A. Grajcar, W. Borek, Influence of hot-working conditions on a structure of high-manganese austenitic steels, *Journal of Achievements in Materials and Manufacturing Engineering* 29 (2008) 139-142.
- [6] A. Grajcar, M. Opiela, G. Fojt-Dymara, The influence of hot-working conditions on a structure of high-manganese steel, *Archives of Civil and Mechanical Engineering* 9/3 (2009) 49-58.
- [7] L.A. Dobrzański, A. Grajcar, W. Borek, Microstructure evolution and phase composition of high-manganese austenitic steels, *Journal of Achievements in Materials and Manufacturing Engineering* 31 (2008) 218-225.
- [8] Y.G. Kim, Y.S. Park, J.K. Han, Low temperature mechanical behavior of microalloyed and controlled-rolled Fe-Mn-Al-C-X alloys, *Metallurgical and Materials Transactions* 16A (1985) 1689-1693.
- [9] C.J. Altstetter, A.P. Bentley, J.W. Fourine, A.N. Kirkbridge, Processing and properties of Fe-Mn-Al alloys, *Materials Science and Engineering A* 82 (1986) 13-25.
- [10] Y.S. Zhang, X.M. Zhu, Electrochemical polarization and passive film analysis of austenitic Fe-Mn-Al steels in aqueous solutions, *Corrosion Science* 41 (1999) 1817-1833.
- [11] M. Opiela, A. Grajcar, W. Krukiewicz, Corrosion behaviour of Fe-Mn-Si-Al austenitic steel in chloride solution, *Journal of Achievements in Materials and Manufacturing Engineering* 33/2 (2009) 159-165.

- [12] M.B. Kannan, R.K.S. Raman, S. Khoddam, Comparative studies on the corrosion properties of a Fe-Mn-Al-Si steel and an interstitial-free steel, *Corrosion Science* 50 (2008) 2879-2884.
- [13] A.S. Hamada, Manufacturing, mechanical properties and corrosion behaviour of high-Mn TWIP steels, *Acta Universitatis Ouluensis C281* (2007) 1-51.
- [14] I.M. Ghayad, A.S. Hamada, N.N. Girgis, W.A. Ghanem, Effect of cold working on the aging and corrosion behaviour of Fe-Mn-Al stainless steel, *Steel Grips* 4 (2006) 133-137.
- [15] A. Grajcar, S. Kołodziej, W. Krukiewicz, Corrosion resistance of high-manganese austenitic steels, *Archives of Materials Science and Engineering* 41/2 (2010) 77-84.
- [16] L. Bracke, G. Mertens, J. Penning, B.C. De Cooman, M. Liebeherr, N. Akdut, Influence of phase transformations on the mechanical properties of high-strength austenitic Fe-Mn-Cr steel, *Metallurgical and Materials Transactions* 37A (2006) 307-317.
- [17] J. Flis, Hydrogen and corrosion degradation of metals, National Science Publishers, Warsaw, 1979 (in Polish).
- [18] M. Opiela, Hydrogen embrittlement of welded joints for the heat-treatable XABO 960 steel heavy plates, *Journal of Achievements in Materials and Manufacturing Engineering* 38/1 (2010) 41-48.
- [19] J. Ćwiek, Hydrogen degradation of high-strength steels, *Journal of Achievements in Materials and Manufacturing Engineering* 37/2 (2009) 193-212.
- [20] S. Prowans, Physical metallurgy, National Science Publishers, Warsaw, 1988 (in Polish).
- [21] G. Wranglen, An introduction to corrosion and protection of metals, Royal Institute of Technology, Stockholm, 1972.
- [22] R.A. Cottis, Stress corrosion cracking, Corrosion and Protection Centre, UMIST, Teddington, 1982.
- [23] P. Kumar, R. Balasubramaniam, Determination of hydrogen diffusivity in austenitic stainless steels by subscale microhardness profiling, *Journal of Alloys and Compounds* 255 (1997) 130-134.
- [24] J. Xu, X. Sun, X. Yuan, B. Wei, Hydrogen permeation and diffusion in low-carbon steels and 16Mn steel, *Journal of Materials Science Technology* 10 (1994) 92-96.
- [25] J. Kittel, V. Smanio, M. Fregonese, L. Garnier, X. Lefebvre, Hydrogen induced cracking (HIC) testing of low alloy steel in sour environment: Impact of time of exposure on the extent of damage, *Corrosion Science* 52 (2010) 1386-1392.
- [26] J. Ćwiek, Hydrogen degradation of high-strength weldable steels, Gdańsk University of Technology Publishers, Gdańsk, 2006 (in Polish).